Influence of computing magnetic field on thermal performance of a magnetocaloric cooling system

Amine Mira[1], **Christophe Espanet**[1], **Thierry de Larochelambert**[1], **Stefan Giurgea**[2], **Philippe Nika**[1]

1. FEMTO-ST Institute, University of Franche-Comte
2 av. Jean Moulin, 90000 Belfort, France
{mohamed_amine.mira; christophe.espanet , philippe.nika @univ-fcomte.fr; thierry.de-larochelambert@femto-st.fr

2. FEMTO-ST Institute, University of Technology of Belfort-Montbéliard
Rue Thierry Mieg, 90000 Belfort, France
stefan.giurgea@utbm.fr

ABSTRACT. *Based on the magnetocaloric effect in some ferromagnetic materials around the room temperature, the magnetic refrigeration is an emerging technology having the following strong advantage comparing to the conventional ones: this technology offers an environmental advantage with avoiding greenhouse gas emissions from refrigerants used in the classical vapor compression machines. However, cost and efficiency have still to be improved. Then, in order to propose an accurate modeling of magnetic refrigeration systems, a multi-physics model is proposed. It consists in coupling a 3D FEM magnetostatic model, an analytic magnetocaloric model and a thermo-fluidic model solved with finite difference method. An analysis of the magnetic field computation evaluates the impact of error on the thermal performances of the system when bypassing 3D FEM.*

RÉSUMÉ. *La réfrigération magnétique est une technologie émergente qui présente des avantages considérables par rapport aux technologies de réfrigération classiques. Basée sur l'effet magnétocalorique de certains matériaux ferromagnétiques autour de la température ambiante, elle offre d'importants avantages environnementaux : d'une part, l'efficacité théorique des cycles utilisés est supérieure à celle des technologies classiques et d'autre part, son fonctionnement n'utilise pas de gaz/vapeur à fort effet de serre comme ceux utilisés dans les machines classiques de compression de vapeur (HFC, HCFC, CFC, etc.). En revanche des verrous scientifiques restent à lever : choix et disposition des matériaux, efficacités d'échanges thermiques et de cycles, gestions des écoulements alternés, coûts. Dans le but de proposer une modélisation précise des systèmes de réfrigération magnétique, un modèle multi-physique est proposé. Il consiste à assembler un modèle 3D magnétostatique résolu par la méthode des éléments finis, un modèle magnétocalorique analytique et un modèle thermo-fluidique résolu par méthode des différences finies. Une analyse de la précision de calcul du*

champ magnétique a été accomplie afin d'évaluer l'impact de l'erreur du calcul du champ magnétique sur les performances thermiques du système.

KEYWORD: *numerical model, magnetocaloric effect, magnetic refrigeration, magnetic field computing.*

MOTS-CLÉS : *modèle numérique, effet magnétocalorique, réfrigération magnétique, calcul magnétique.*

DOI:10.3166/EJEE.17.151-170 © Lavoisier 2014

1. Introduction

The worldwide cooling production energy represents in average more than 15% of the total electrical energy consumption (Coulomb, 2005). Mainly, the cooling is based on the conventional technology, *i.e.* vapor compression systems. Despite a severe ODP standard concerning vapor/gas (Montréal Protocol), most of vapor compression systems use greenhouse gases such as HFCs.

The magnetic refrigeration is a promising alternative to classical refrigeration systems since this technology presents many advantages (Kedous-Lebouc *et al*., 2005): the global environmental impact is lower, indeed greenhouse gases are not used, the theoretical refrigeration efficiency is higher and the noise is reduced (working without a compressor).

The magnetic refrigeration is an emerging technology; several laboratories have been interested in this field and have confirmed the working principle with designing and realizing prototypes. The first prototype of magnetic refrigeration was built in 1976, aiming at reaching the lowest possible temperature for cryogenics applications (Gschneidner, Pecharsky, 2008). The first prototypes using magnetic refrigeration at room temperature were designed in the end of 90's and several technologies were tested to optimize thermal performances.

However several drawbacks remain to be eliminated in order to pretend for household or automotive applications. Indeed, technological and economic barriers are still to overcome, e.g. thermal power and temperature difference achieved by the latest prototypes are not yet comparable to those using conventional technology; moreover the cost of magnetocaloric materials is still high.

In the aim of improving performances of magnetic refrigeration systems, accurate modeling of magnetic, magnetocaloric and thermal phenomena is essential. For this purpose several models have been proposed in the literature to include the maximum of these phenomena (Nielsen *et al*., 2011; Roudaut *et al*., 2011).

Different ways to take into account the local magnetic field are used in the literature but the importance given to the exact modeling of magnetic field seems not always essential, because of frequently simplified boundary conditions, use of magnetocaloric experimental curves such as ΔT_{ad} curves and imposed magnet external field, avoiding time consuming computations.

In this paper, we propose firstly a brief presentation of the magnetic refrigeration: composition of magnetic refrigerator systems, working principle and some prototypes performances. Then, the multi-physics model is presented and applied to the test bench developed in our laboratory. Relevant results are described to highlight the influence of magnetic computation on the magnetic refrigeration; the different ways to take into account the magnetic phenomena are described as long as errors occurring when magnetic field values are imposed in the calculation of thermal power.

2. Presentation of magnetic refrigeration

The magnetic refrigeration is based on the magnetocaloric effect (MCE) in some materials around room temperature.

The magnetocaloric effect is based on the critical transition paramagnetic/ ferromagnetic of magnetic materials (Figure 1): any change in external magnetic field around their Curie temperature induces a reversible change in their correlated electronic spin entropy, directly related to strong specific thermal power production/absorption (Tishin *et al.,* 1999). When these magnetization changes occur in an adiabatic way, they produce the so-called adiabatic temperature change, ΔT_{ad} which is a function of magnetic field and initial temperature.

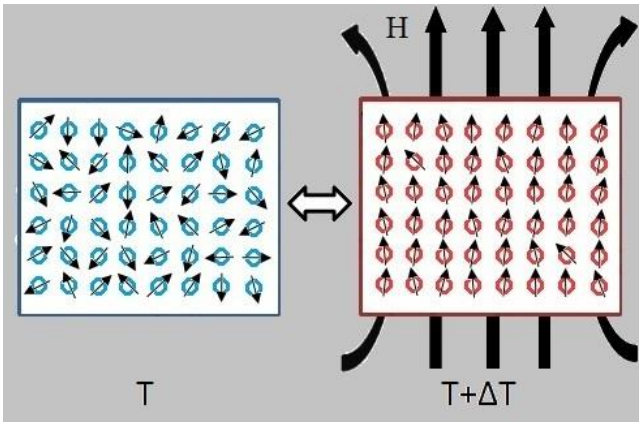

Figure 1. Magnetocaloric effect principle

The maximum magnetocaloric effect occurs at a temperature close to the Curie temperature of the material, slightly depending on the external magnetic field. For the record, the Curie temperature T_c characterizes the thermodynamic state point at which magnetic second order critical transition occurs, *i.e.* spontaneous

magnetization/demagnetization (atomic spin ordering/disordering) without external magnetic field while varying temperature under/above T_c.

In order to apply the magnetocaloric effect to magnetic refrigeration, magnetic materials with Curie temperatures around room temperature are very useful. Among these, rare earth elements such as *gadolinium* and some of its alloys show the highest MCE (Yu *et al*., 2003) but still remain expensive. More recently, new *lanthanum* alloys encounter increasing interest because of their rather good magnetocaloric properties and lower prices (Bjørk *et al*., 2010).

Besides magnetic materials, magnetic refrigeration systems need fluid coolants which transfer heat between magnetocaloric materials and heat sources (tanks) through adequate exchangers after magnetization/demagnetization phases (towards hot/cold tank, respectively).

The magnetic field is created by different ways: superconductor to reach great magnetic field intensity, permanent magnet (most used) for compact systems and electromagnet for static academic systems. As the superconductors must be cooled, it compromises its application to magnetic refrigeration at small scale. The use of rare earth permanent magnets enable to design very compact systems, but the cost of such magnets is high. The electromagnet is not sufficient for high levels of magnetic flux intensity, but it could be useful for experimentation, because the control of magnetic field is easy.

Generally, the temperature variation simply induced by magnetocaloric effect is not large enough to allow for refrigeration. In order to amplify the temperature span, the magnetic material has to be submitted to magneto-thermodynamic cycles. Several thermodynamic cycles can be applied in magnetic refrigeration systems (Romero Gómez *et al*., 2013) such as Carnot, Brayton, Ericsson and Active magnetic regenerator cycles. The Active Magnetic Regenerator cycle (AMR) is the most used in the magnetic refrigeration prototypes, because the magnetic material is useful not only to provide the temperature change (specific magnetocaloric heat power), but also to work as a regenerator for the heat transfer flow towards heat sources (active heat storage and memory as though as heat exchanger).

More precisely, the AMR cycle consists of four phases (Figure 2):

a) the material is adiabatically magnetized and heats (temperature increases);

b) the coolant fluid flows through the material from the cold to the hot tank while keeping magnetic field constant (cold blow);

c) the material is adiabatically demagnetized and cools (temperature decreases);

d) the coolant fluid flows through the material from the hot to the cold tank while keeping magnetic field constant (hot blow).

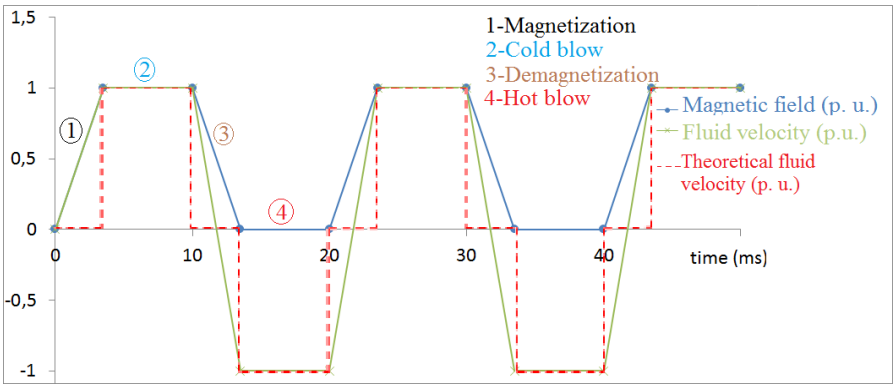

Figure 2. AMR cycles phases

Since the magnetic refrigeration principle was proven, several prototypes were built in some laboratories in the world. Although the first prototype was designed for cryogenic application in 1933, the first prototype for refrigeration applications has only been built in 1976 and numerous others have been built since the late 90's (Yu *et al.*, 2010). Recently, the Risø DTU (Denmark) prototype has reached a cooling power of 1 kW, however with zero temperature span (Bahl *et al.*, 2013). Many efforts should be made to further increase both magnetic refrigeration systems power and temperature span. Among several solutions, one is the use of regenerators composed of different materials showing close but different Curie temperature (Legait *et al.*, 2014).

3. Description of the test bench developed at FEMTO-ST Institute

In the context described in the previous section, a fundamental experimental magnetocaloric test bench is currently in development in our laboratory (FEMTO-ST Institute). In this system, the magnetic field is produced by an electromagnet that we have designed specifically for this bench (Figure 3a) with particularly restricting specification:

– a traversing hole has been managed right through the magnetic core to introduce laser beams and camera lenses for µPIV measurements in alternating flows inside regenerators;

– a rigid wide air gap (21 mm) has been imposed for the regenerators to take place;

– a quite constant uniform 1 T magnetic induction can be periodically produced during very short times (3,5 ms) in the air gap during magnetization phases.

Table I summarizes electromagnet dimensions. The distribution of the magnetic field in the air gap without magnetocaloric regenerator is shown on Figure 3b (The

homogeneity of magnetic flux density can be observed the central zone of the central cross section), Figure 3c (axial magnetic flux density profile along the center line in the air gap), the magnetic field is obtained by a finite element software (Flux3D).

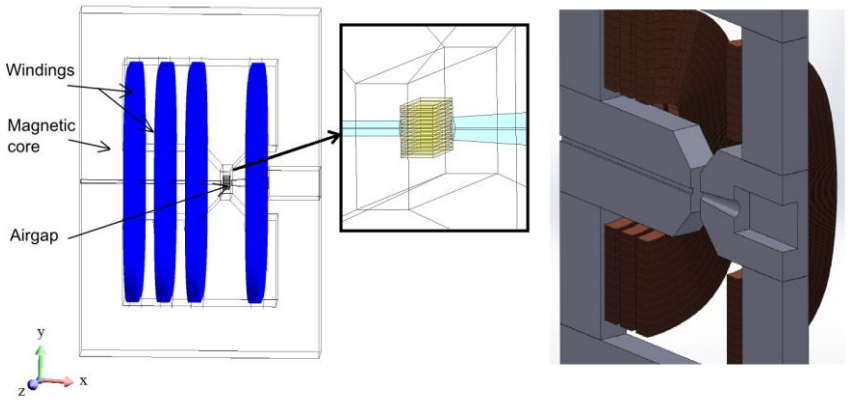

Figure 3a. Magnetic field source used in the laboratory test bench

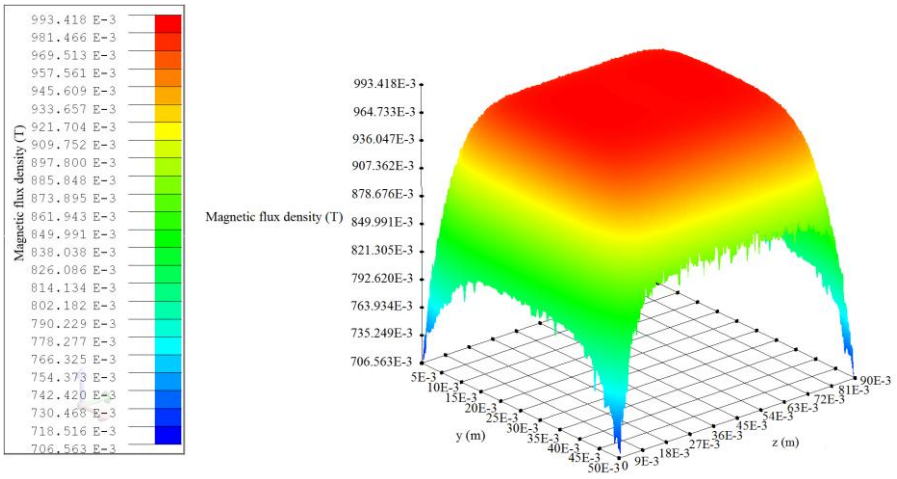

Figure 3b. Magnetic flux density in central cross section of air gap

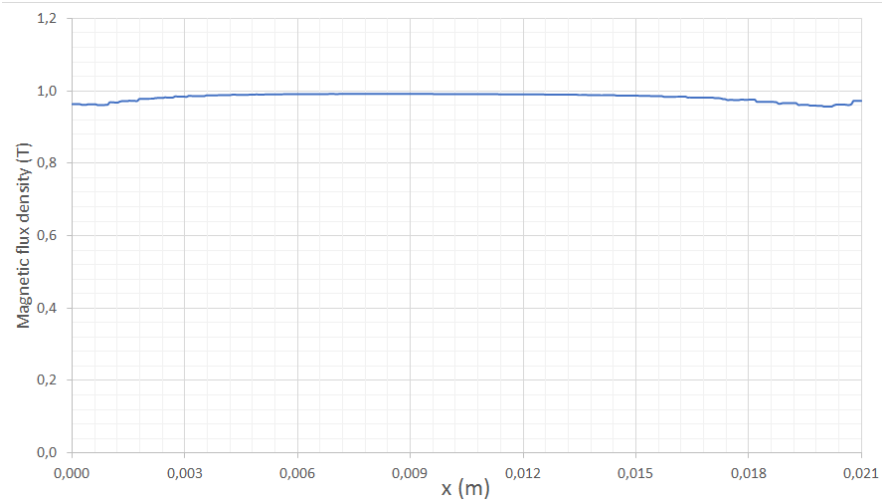

Figure 3c. Axial magnetic flux density profile along the center line in the air gap

Table 1. Electromagnet dimensions

Dimensions	**Values**
Length	500 mm
Height	600 mm
Depth	90 mm
Air gap width	21 mm
Air gap height	50 mm

The electric current in the windings is provided by an inverter limited to 50 A for each coil in order to respect a maximum current density corresponding to maximum Joule heating. Indeed, too high heating would disturb heat balance in AMR cycles and imply less efficiency of the system. The current is controlled in order to achieve the AMR cycle specification (Figure 4).

The regenerator comprises 13 *gadolinium* plates (1 mm ×13 mm ×45 mm) and is placed at the center of the electromagnet air gap. The coolant fluid (Zitrec-S10) flows between the plates in order to exchange heat alternatively with hot and cold tanks through micro-exchangers. Fluid flow and magnetic field are synchronized to achieve an AMR cycle (Figure 2).

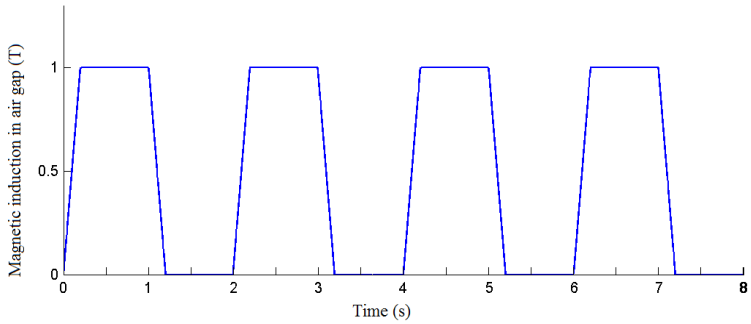

Figure 4. Required magnetic induction in the air gap for AMR cycle functioning (ex. 0.5 Hz frequency)

4. Multi-physics modeling

In parallel with the design and the construction of the test bench, a multi-physics model have been developed in the laboratory to simulate, step by step, the AMR cycle as shown in Figure 5. To do that, the whole system model can be divided into three sub-models: a magnetostatic model, a magnetocaloric model and a thermo-fluidic model. The coupling of these three sub-models is coded into a single program with Python 2.7.2. The sub-models are presented in the next subsections.

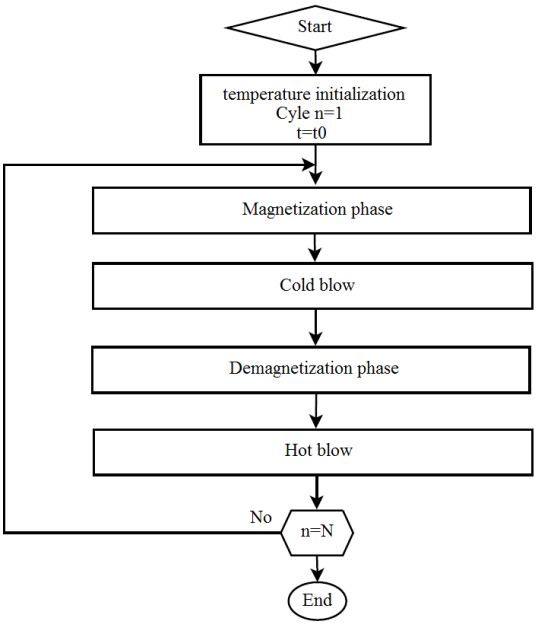

Figure 5. AMR cycle simulation strategy

4.1. Magnetostatic model

The magnetostatic model requires the value of the electrical current in the windings of electromagnet (the magnetic source) and $B(H,T)$ characteristic of the magnetocaloric material (*gadolinium*), where $H=H_{appl}-N_dM$ stands for the internal magnetic field, H_{app} being the applied magnetic field, N_d and M the demagnetizing factor and magnetization of the gadolinium sample. As shown in Figure 6, the *gadolinium* shows particular thermophysical properties depending on its temperature along with external magnetic field and exhibits a ferromagnetic behavior for temperatures below 293 K, becoming paramagnetic above 293 K (critical transition). These curves have been calculated from the magnetization data $M(H_{app}, T)$ in (Allab *et al.*, 2006) after correction for demagnetization (de Larochelambert, n. d.).

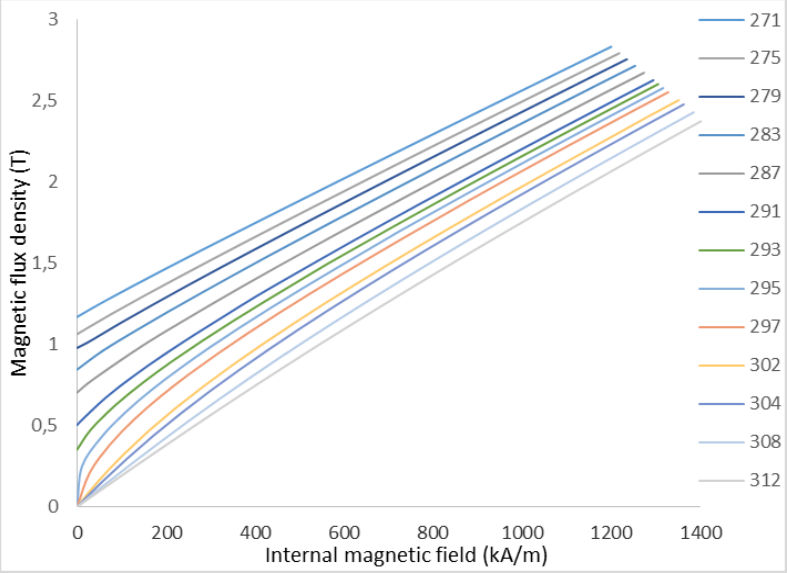

Figure 6. B(H,T) characteristics of the gadolinium as a function of temperature

Therefore, before each magnetic resolution, an interpolation has to be done according to the temperature of the material, in order to determine the $B(H)$ curve of the material, then, the magnetostatic Equations (1-3) is solved with a 3D finite element software (Flux3D®)(Cedrat, 2012).

$$\nabla \times H = J \tag{1}$$

$$H = -\nabla \phi_{red} + H_j \tag{2}$$

$$\nabla \bullet \left(\mu_0 \cdot [\mu_r] \cdot \left(-\nabla \phi_{red} + H_j\right) + B_r\right) = 0 \tag{3}$$

where H_j, $\prod_{red}$ and B_r are the magnetic field of the windings (Biot – Savart law), reduced magnetic potential and remanent magnetic induction respectively. The outputs of this model are the different values of magnetic field in the regenerator.

This model is flexible, *i.e.* the model can easily be adapted for other sources of magnetic field such as permanent magnets, Halbach cylinders etc.

4.2. The magnetocaloric model

The thermal power density produced in the magnetocaloric material during magnetic field variations is calculated with (4) (Weiss 1921), which requires the magnetic field calculated by the first sub-model.

$$\dot{q} = -\mu_0 \cdot T \cdot \left(\frac{\partial M}{\partial T}\right)_H \cdot \frac{dH}{dt} \tag{4}$$

where T, M and H are the temperature, magnetization and local internal magnetic field intensity respectively.

We determine the magnetization by interpolation from the experimental measurement data (Allab *et al*., 2006) according to local internal magnetic field and temperature values (Figure 7) using magnetocaloric equation of state to correct for demagnetizing field (de Larochelambert, n.d.). In this study, the author uses a critical thermodynamic approach based first on relevant non-dimensional magnetization and temperature relative to critical behavior and exponents that must converge at critical values, and second on the analogy with the critical vapor-liquid transition following all symmetries and symmetry breaking constraints of universal laws for free energy and its first and second derivatives. This model leads to a single curve representing the magnetization of *gadolinium* in a large domain of internal magnetic field H_{int} and temperature T around its critical point by fitting precisely all critical exponents and demagnetization factor N_d of the sample used for experimental measurements. The local magnetization gradient is deduced, allowing for calculation of the local magnetocaloric power production. This calculation of the MCE is the so-called “built-in method” (Nielsen *et al.,* 2011).

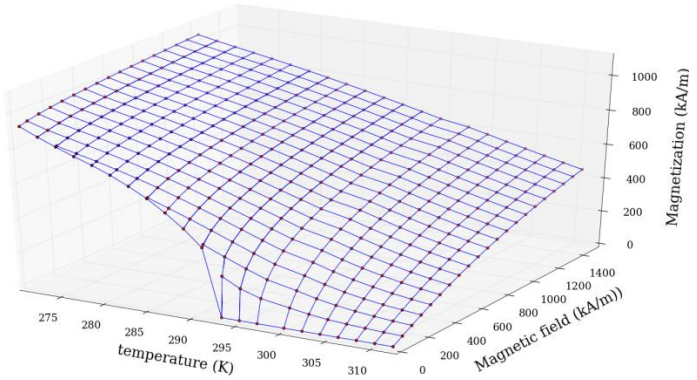

Figure 7. Calculated magnetization of the gadolinium as a function of temperature and internal magnetic field

4.3. Thermo-fluidic model

The thermo-fluidic model is based on a 1D model in the fluid flow direction *z* (Figure 8). The following equations (Engelbrecht, 2008) describe the thermal behavior of a fluid particle (subscripts: f) and a magnetocaloric material element (subscripts: m).

$$\begin{cases} m_f \cdot C_f \cdot \left(\dfrac{\partial T_f}{\partial t} + V(t) \cdot \dfrac{\partial T_f}{\partial z} \right) = h(t) \cdot S \cdot (T_m - T_f) \\ m_m \cdot C_p(H, T_m) \cdot \dfrac{\partial T_m}{\partial t} - \lambda \cdot v \cdot \dfrac{\partial^2 T_m}{\partial z^2} = \dot{q} \cdot v + h(t) \cdot S \cdot (T_f - T_m) \end{cases} \tag{5}$$

where T, h, S, λ, v, $\dot{q}$, m, C, V indicate temperature, convection coefficient, exchanging surface, thermal conductivity, solid cell volume, magnetocaloric power density, mass, specific heat capacity and fluid velocity respectively.

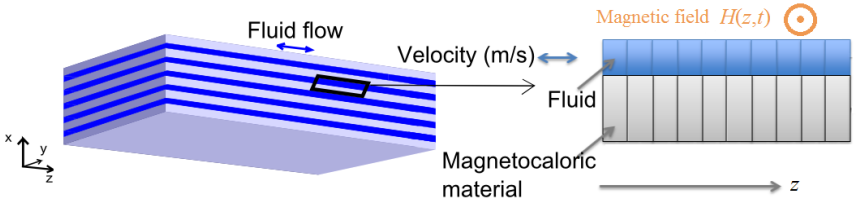

Figure 8. 1D model for the thermal model

The heat exchange coefficient *h* has been obtained otherwise by an analytical method (de Larochelambert, Nika, n.d.). In this paper, the authors solve the conservation equations of mass, momentum and energy in alternating fully-developed flows between parallel plates with established wall temperature gradient, by means of Laplace transform. The time evolution of the flow velocity and temperature is obtained after inversion of the Laplace transform solutions by means of the residue theorem, leading to new friction $Cf(Re_{max}, Wo)$ and heat transfer Nu_{RMS} (Re_{max}, Wo) correlations, Re_{max} and Wo being the maximum Reynolds number and the Womersley number of alternating flow in the channel. The heat exchange coefficient *h* in Equation (5) is thus calculated from the Nu_{RMS} value.

In the same way, the well-known experimental data of the heat capacity of *gadolinium* (Dan'kov *et al.,* 1998) are first corrected for demagnetization and then used to precisely calculate the value of the specific heat capacity of *gadolinium* for each temperature and internal magnetic field calculation point using interpolation method.

The 1D energy Equation (5) in the fluid uses the imposed value of the bulk fluid velocity $V(t)$ in each channel during the cold and hot blow, which is calculated from incompressible fluid volume conservation, cold/hot blow time duration and discharge ratio (α = swept volume/channel volume) of the channels. This theoretical sequence $V(t)$ is the same as the real one by means of a position controlled hydraulic cylinder.

In order to solve these coupled equations, a finite difference method with explicit scheme has been used and coded with Python; the Courant-Friedrich-Levy criterion ($V \cdot \Delta t / \Delta z < 1$ where Δt, Δz are the time step and spatial discretization element, respectively) is tested to ensure convergence of the model (Courant *et al.,* 1967). The ambient temperature is taking as initial condition and the hot and cold tank temperatures as space limit conditions.

5. Coupling strategy and results

The coupling of the three sub-models is coded into a single program. The coupling strategy is the following order:

1. according to time and temperature, each magnetocaloric $B_T(H)$ curve of *gadolinium* is interpolated and then defined in Flux3D software, which is driven by Python code to solve magnetic equations;

2. according to the obtained internal magnetic field in the middle of each segment of the central plate of the *gadolinium* (according to the thermal mesh), local magnetization is deduced at current temperature, and then local magnetocaloric heat power density is calculated;

3. temperatures are computed according to the heat diffusion in the material and heat convection in the fluid, and these temperatures are returned to the first step; the time is incremented.

Finally, we have two ways to take into account the magnetostatic model:

– coupling Flux3D software, to accurately compute local magnetic field distribution in the regenerator. The main drawback of this approach is the large calculation time, due to the call of the FEM software at each time step to solve the magnetostatic equations; however, taking into account the local distribution of the magnetic field enables more realistic results;

– imposing a perfect trapezoidal magnetic field shape (homogenous value of magnetic field in the regenerator) assuming a perfect demagnetization of the magnetocaloric material, the main advantage of this method being the gain in computational time.

The multi-physics model with coupling Flux3D software is applied to the test bench described in the section 3. For this calculation, the simulation parameters are summarized in Table 2.

Table 2. Model parameters

Parameters	**Values**
Frequency	0.5 Hz
Number of simulated cycle	25 cycles
Duration of magnetization and demagnetization	3.5 ms
Initial temperature	293 K
Hot source temperature	296 K
Heat capacity of the fluid	3630 J/kg. K
Channel discharge ratio α	100 %
Spatial discretization number	10 points
Gadolinium plate thickness	1 mm
Distance between plates (channel height)	0.5 mm

The boundary conditions are chosen as follows:

– solid-fluid boundaries: convecto-conductive heat flux conservation through the boundaries (last term of Equations (5)). The heat transfer coefficient *h* is calculated by means of the theoretical heat transfer correlation obtained in (de Larochelambert, Nika, n.d.);

– fluid inlet condition in each channel: adiabatic bulk temperature of 10 fluid cells or imposed heat source temperature (two cases);

– fluid outlet condition in each channel: adiabatic bulk temperature of concerned heat source (hot or cold) comprising 10 fluid cells: adiabatic mixing with 10 fluid cells or imposed heat source temperature;

– no thermal conduction in fluid or *gadolinium* (negligible);

– magnetic flux conservation through the whole space volume (magnetic circuit, air, regenerator).

The temperature span produced between the hot and cold side of the regenerator is shown in Figure 9. The steady state is almost reached after 70 cycles, and a temperature span of 5.3 K between the cold tank and the imposed hot source is obtained for these simulation parameters (these parameters can be further optimized to amplify the temperature span). These results illustrate the working of the coupled models and predict the behavior of the system. They will be compared to experimental results in a next paper.

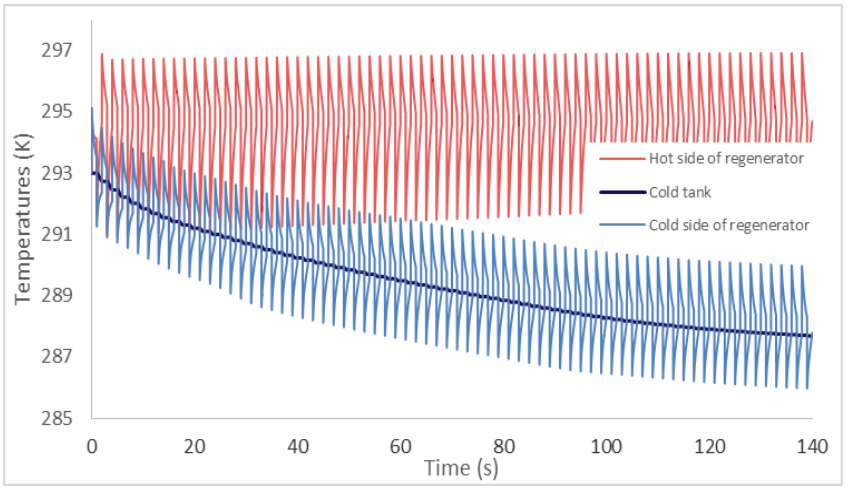

Figure 9. Time evolution of hot and cold tanks temperatures

Figure 10 shows the obtained magnetic field which is slightly different along the plate because of the 3D effect and the *B*(*H*) behavior depending on the temperature. One can observe the four phases of the AMR cycle (production ramp of high magnetic field – constant magnetic field – magnetic field removal – constant magnetic field). As shown in the zoom frames, during the magnetization state, the magnetic field is impacted by the temperature (around 6%) indeed; the cold side allows passing more flux lines than the hot side because both permeability and magnetization decrease while increasing temperature. However this effect is compensated by the demagnetizing field and the flux leakage at the end of the regenerator which are important with high magnetization. During the

demagnetization state *i.e.* when applied field is zero, as the model takes into account the real $B(H)$ curve of the *gadolinium*, the obtained internal magnetic field is equal to the coercive field which is almost zero. The values of the coercive field of the *gadolinium* are taken from the paper (Döbrich *et al.*, 2012).

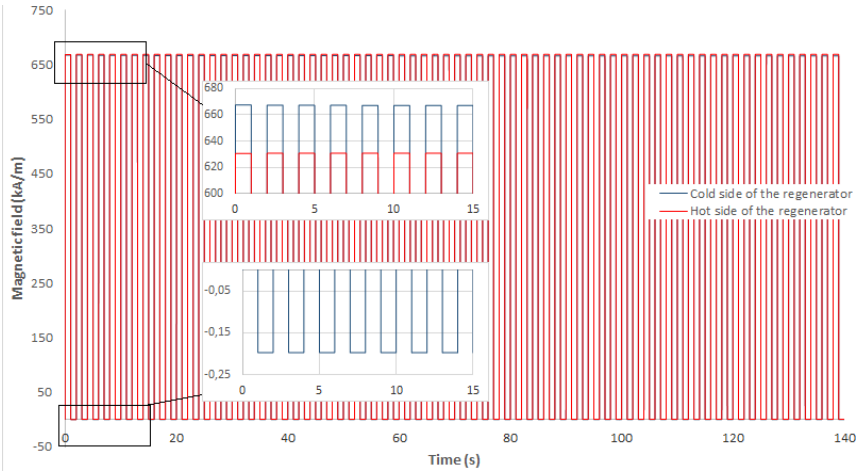

Figure 10. Magnetic field in the regenerator over time obtained by the coupled model

6. Influence of computing magnetic field

In this part, we propose to study the influence of the knowledge of magnetic field local distribution. We compare resulting temperatures and cooling power by using the model with computing the local magnetic field, *vs.* with imposed internal magnetic field.

This comparison is particularly meaningful if we keep in mind that the former calculation is rather time consuming compared to the latter. For instance, computing one stable working point of the whole magnetocaloric system needs 13 min per cycle when computing local magnetic field and 1.51 min per cycle when imposing uniform magnetic field. These computations time were estimated on an Intel Xeon CPU E3-1270 3.40 GHz processor.

6.1. Influence of computing magnetic field on temperatures

Firstly, we compare the impact of the imposed method on the temperature span reached between the hot (imposed at 296 K) and cold tanks. As shown in the Figure 11 an important error of more than 1.3 K between the temperature spans calculated by the two methods can be observed.

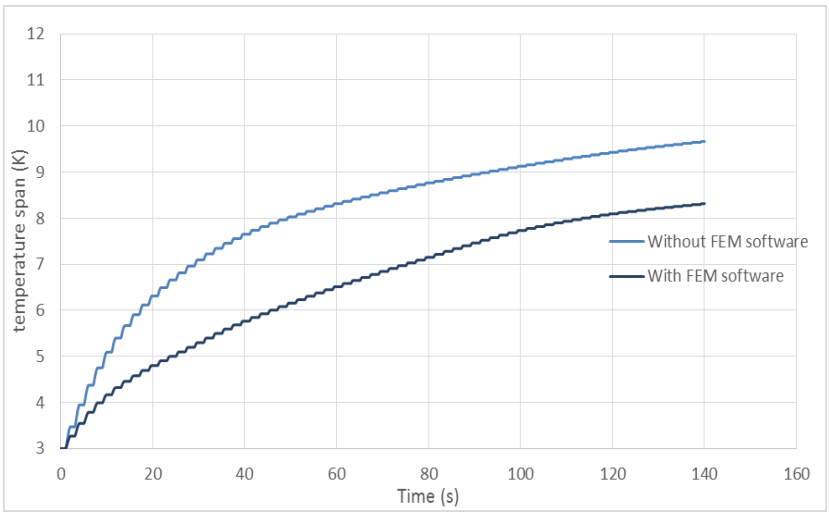

Figure 11. Time evolution of the temperature span for the two methods

This difference can be explained by the fact that imposed model assumes a perfect demagnetization of the *gadolinium* plate *i.e.* imposing a zero internal magnetic field in all parts of the regenerator; thus during the demagnetization, the produced magnetocaloric power is higher, the derivative of the magnetization in respect to temperature and internal magnetic field being overestimated due to the linear interpolation of the $M(H, T)$ data. The coupling model with FEM software takes into account the inhomogeneity of magnetic field in the regenerator, the demagnetizing field and 3D effects, so that the results involve these corresponding energy drops and are more realistic.

6.2. Influence of computing magnetic field on the cooling power

In this part, we study the direct impact of the magnetic field calculation on the cooling power transferred to the cold tank; this power is computed with using (6) based on the heat transmitted from the fluid exiting from outlets during the hot blow to the cold tank and considering a perfect exchanger.

$$P_f(t) = \sum_{1}^{N} m_{ex} \cdot c_p(t) \cdot \frac{\Delta T}{\Delta t} = N \cdot m_{ex} \cdot c_p(t) \cdot \frac{T_{ct}^{\,ti+1} - T_{fex}^{\,ti}}{\Delta t} \tag{6}$$

in which N, m_{ex}, T_{ct}, T_{fex} are the number of fluid channels, mass of exiting fluid, cold tank and exiting fluid temperatures, respectively.

This study consists in carrying out a series of simulation and determining the curve of the cooling power as a function of the temperature span imposed between tanks. The results shown in Figure 12 demonstrate that cooling power is higher for lower temperature spans and it decreases monotonically with imposed temperature span.

The calculated cooling power is also overestimated when imposing homogeneous internal magnetic field for a given temperature span; this is the results of accumulation of minor errors from the beginning of the cycle: very little differences of internal magnetic field induce small differences in magnetization values that lead to bigger differences in magnetocaloric power densities around Curie temperature. This in turn produces larger temperature variations (temperatures of fluid and magnetocaloric material) that generate further magnetization deviations, therefore internal magnetic field, etc. In addition, these errors are amplified when computing cooling power because of their duplication on all the 13 channels according to Equation (6).

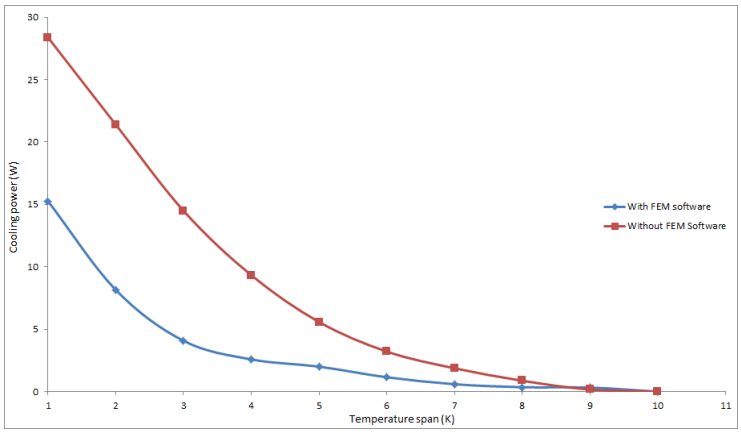

Figure 12. Cooling power as a function of temperature span with two magnetostatic methods (0.5 Hz frequency)

To keep the accuracy of the coupling model, it is necessary to use a consistent data and well-suited interpolation methods of magnetization of the magnetocaloric material as a function of temperature and internal magnetic field (Risser *et al.*, 2012). Another way of improving the accuracy of calculation is the use of bi-cubic interpolation of the magnetization M (H, T) and heat capacity C_p (H, T); this will be presented in a next paper.

7. Conclusion

A numerical model of an AMR system has been developed; the model considering the multi-physics phenomena of magnetic refrigeration simulates both the magnetocaloric material behaviors and the AMR cycle with local produced magnetic field. This model is applied to a test bench that has been developed at FEMTO-ST Institute considering some assumptions such as 1D modelling to represent thermo-fluidic phenomena or neglecting thermal diffusion in the regenerator; the aim is to predict the magnetic and thermal performances of the system. The multi-physics model allows to determine spatial and temporal distribution of local magnetic field, magnetocaloric power density created in each part of the regenerator, and temperature distribution in the regenerator and in the coolant fluid.

The influence of magnetic field computing on thermal performances has been assessed; as a result the error committed by neglecting magnetic phenomena as well as demagnetizing field, 3D effects and dependence of magnetocaloric material properties on temperature span has been calculated. It has been found that this error is more important when calculating the cooling power.

Despite very important calculation time, taking into account local magnetic field calculation allows more realistic results.

This model will be compared for validation with the data obtained from the experimental test bench in a next paper and further be used to increase the thermal power by optimizing AMR cycle parameters.

Bibliography

Allab F., Kedous-Lebouc A., Yonnet J.P., Fournier J.M. (2006). A magnetic field source system for magnetic refrigeration and its interaction with magnetocaloric material. *International Journal of Refrigeration*, vol. 29, n° 8, p. 1340-1347.

Bahl C.R.H., Engelbrecht K., Eriksen D., Lozano J.A., Bjørk R., Geyti J., Nielsen K.K., Smith A., Pryds N. (2014). Development and experimental results from a 1 kw prototype AMR. *International Journal of Refrigeration*, 37, p.78-83.

Bjørk R., Bahl C.R.H. & Katter M. (2010). Magnetocaloric properties of LaFe13−x−yCoxSiy and commercial grade Gd. *Journal of Magnetism and Magnetic Materials*, vol. 322, n° 24, p. 3882-3888.

Cedrat (2012). *Guide d'utilisation Flux 11* vol. *3*, Grenoble.

Coulomb D. (2005). Health and environment: The two key IIR challenges. In *Magnetic Refrigeration at Room Temperature*. Montreux, Switzerland.

Courant R., Friedrichs K., Lewy H. (1967). On the Partial Difference Equations of Mathematical Physics. *IBM Journal of Research and Development*, vol. 11, n° 2, p. 215-234.

Dan'kov S., Tishin A.M., Pecharsky V.K., Gschneidner Jr. (1998). Magnetic phase transitions and the magnetothermal properties of gadolinium. *Physical Review B*, vol. 57, n° 6, p. 3478-3490.

Döbrich F., Kohlbrecher J., Sharp M., Eckerlebe H., Birringer R. & Michels A. (2012). Neutron scattering study of the magnetic microstructure of nanocrystalline gadolinium. *Physical Review B*, vol. 85, n° 9, p. 1- 17.

Engelbrecht K. (2008). *A Numerical Model of an Active Magnetic Regenerator Refrigerator with Experimental Validation*. PhD thesis, University of Wisconsin-Madison.

Gschneidner K.A., Pecharsky V.K. (2008). Thirty years of near room temperature magnetic cooling: Where we are today and future prospects. *International Journal of Refrigeration*, vol. 31, n° 6, p. 945-961.

Kedous-Lebouc A., Allab F., Fournier J.M., Yonnet J.P. (2005). Réfrigération magnétique. *Techniques de l'ingénieur*, RE 28-1(0), p. 0-16.

De Larochelambert T. (To be published). Looking for a magnetic equation of state of gadolinium.

De Larochelambert T., Nika P. (Submitted). Heat transfer and friction coefficients in alternating flows between parallel plates for magnetocaloric regnerators. *International Journal of Thermal Sciences.*

Legait U., Guillou F., Kedous-Lebouc A., Hardy V., Almanza M. (2014). An experimental comparison of four magnetocaloric regenerators using three different materials. *International Journal of Refrigeration*, 37, p.147-155.

Nielsen K.K., Tusek J., Engelbrecht K., Schopfer S., Kitanovski A., Bahl C.R.H., Smith A., Pryds N., Poredos A. (2011). Review on numerical modeling of active magnetic regenerators for room temperature applications. *International Journal of Refrigeration*, vol. 34, n° 3, p. 603-616.

Risser M., Vasile, C., Keith B., Engel T., Muller C. (2012). Construction of consistent magnetocaloric materials data for modelling magnetic refrigerators. *International Journal of Refrigeration*, vol. 35, n° 2, p. 459-467.

Romero Gómez J., Ferreiro Garcia R., De Miguel Catoira A., Romero Gómez M. (2013). Magnetocaloric effect: A review of the thermodynamic cycles in magnetic refrigeration. *Renewable and Sustainable Energy Reviews*, 17, p. 74-82.

Roudaut J., Kedous-Lebouc A., Yonnet J.P., Muller C. (2011). Numerical analysis of an active magnetic regenerator. *International Journal of Refrigeration*, vol. 34, n° 8, p. 1797-1804.

Tishin A., Gschneidner K.A., Pecharsky V.K. (1999). Magnetocaloric effect and heat capacity in the phase-transition region. *Physical Review B*, vol. 59, n° 1, p. 503-511.

Weiss P. (1921). Le phénomène Magnéto-Calorique. *Le journal de la physique et le Radium*, p. 161-182.

Yu B., Liu M., Egolf P.W., Kitanovski A. (2010). A review of magnetic refrigerator and heat pump prototypes built before the year 2010. *International Journal of Refrigeration*, vol. 33, n° 6, p. 1029-1060.

Yu B., Gao Q., Zhang B., Meng X.Z., Chen Z. (2003). Review on research of room temperature magnetic refrigeration. *International Journal of Refrigeration*, vol. 26, n° 6, p. 622-636.

Received: 7 January 2014
Accepted: 17 July 2014